Journal of Manufacturing Processes 172 (2026) 851–863

Contents lists available at ScienceDirect

Journal of Manufacturing Processes

journal homepage: www.elsevier.com/locate/manpro

Mechanism of ultrasonic vibration-assisted solid-state reaction grinding of sapphire

Gen Chen [a,b], Zhongwei Hu [a,b,*], Kun Shi [a,b], Yuqiang Zhang [a,b], Xintian Cai [c], Qing Peng [d,**]

[a] Institute of Manufacturing Engineering, Huaqiao University, Xiamen, China
[b] Institute of Mechanical Engineering and Automation, Huaqiao University, Xiamen, China
[c] School of Mechanical Engineering, Hubei University of Technology, Wuhan, 430068, China
[d] School of Power and Mechanical Engineering, Wuhan University, Wuhan, China

HIGHLIGHTS

- A novel ultrasonic vibration–assisted solid-state reaction grinding method for sapphire is proposed.
- The feasibility of the method is verified by theory and numerical.
- Molecular dunamics reveals the microscopic grinding mechanisms.
- Material removal increases by 10.27-53.45%, while roughness decreases by 17.84-21.91%.

GRAPHICAL ABSTRACT

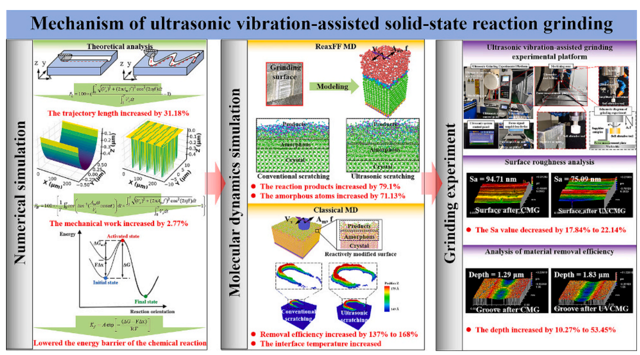

ARTICLE INFO

Keywords:
Ultrasonic vibration-assisted energy field
Sapphire
Solid-state reaction
Molecular dynamics
Grinding mechanism

ABSTRACT

Sapphire is a typical hard and brittle material whose high-efficiency machining remains challenging due to the low material removal rate of chemical mechanical grinding (CMG). To address this limitation, an innovative ultrasonic vibration-assisted CMG (UVCMG) method is proposed by introducing an ultrasonic-assisted energy field to promote interfacial solid-state reactions. Theoretical analysis and numerical modeling demonstrate that ultrasonic vibration provides additional energy input to the interface, thereby facilitating solid-state reactions. Molecular dynamics simulations further reveal enhanced interfacial reactions, increased amorphization, and accelerated removal of reaction-modified atoms. Consistent with these findings, grinding experiments show that UVCMG achieves a 10.27%–53.45% increase in material removal efficiency, a 17.84%–21.91% reduction in surface roughness, and reduced grinding forces compared with CMG. This work provides an efficient and mechanism-informed approach for precision machining of sapphire and other hard and brittle materials.

* Correspondence to: Z. Hu, Institute of Manufacturing Engineering, Huaqiao University, Xiamen, China.
** Corresponding author.
E-mail addresses: huzhongwei@hqu.edu.cn (Z. Hu), pengqing@whu.edu.cn (Q. Peng).

https://doi.org/10.1016/j.jmapro.2026.06.006
Received 8 January 2026; Received in revised form 21 April 2026; Accepted 2 June 2026
Available online 16 June 2026
1526-6125/© 2026 The Society of Manufacturing Engineers. Published by Elsevier Ltd. All rights are reserved, including those for text and data mining, AI training, and similar technologies.

1. Introduction

Sapphire has extensive applications in fields such as aerospace engineering, healthcare technology, electronic products, high-power laser systems, and optical precision devices, owing to its superior optical transparency, excellent dielectric behavior, notable mechanical robustness, and remarkable chemical stability [1–4]. Components fabricated from sapphire demand exceptional surface integrity and machining precision [5–8]. Nevertheless, due to its inherent characteristics of hardness and brittleness, sapphire presents significant challenges during material removal. Grinding is the primary method for achieving rapid material removal from sapphire surfaces [9,10]; however, it inevitably introduces severe surface and subsurface damage [11–15]. To eliminate the damage layer generated by abrasive grinding and obtain high-quality surfaces, chemical mechanical polishing (CMP) is commonly employed. Nevertheless, the material removal efficiency of CMP remains extremely low [16–21].

To achieve both high efficiency and high precision in machining, researchers have proposed the chemical mechanical grinding (CMG) approach. Its core mechanism involves the use of reactive abrasives that chemically interact with the workpiece surface to form a softened reaction layer, which is subsequently removed through mechanical grinding [22,23]. The surface integrity and precision achieved through CMG are comparable to those of CMP, while maintaining excellent geometric accuracy [24–27]. Experiments showed that surface roughness could be reduced to below 1 nm within one hour, indicating the significant potential of CMG for sapphire grinding [28]. Scholars further systematically investigated soft abrasives suitable for sapphire processing. Among five oxides ZnO, SiO_2, MgO, Fe_3O_4, and MnO that exhibit significant chemical reactions with Al_2O_3, SiO_2 was identified as the most suitable soft abrasive for tribochemical polishing of sapphire, based on considerations of abrasive hardness and reaction activation energy [29]. Comparative dry grinding experiments using Cr_2O_3 and SiO_2 wheels respectively showed that both achieved sapphire surface roughness below 1 nm with material removal rates below 1 μm/h. However, in terms of subsurface damage control, SiO_2 abrasives produced damage-free subsurfaces, while Cr_2O_3 abrasives introduced a nearly 100 nm subsurface damage layer, demonstrating the superiority of SiO_2 abrasives over Cr_2O_3 [30]. With ongoing research into abrasive composition, novel wheel formulations for dry CMG of sapphire have been developed, enabling surface finishes under 1 nm and enhancing removal efficiency to around 1.13 μm/h significantly improving machining productivity compared to earlier approaches [31,32]. Overall, although CMG is capable of producing near-perfect sapphire surfaces with negligible subsurface defects, the relatively slow rate of surface reaction between abrasives and sapphire remains a bottleneck for its broader application. The kinetics of interfacial chemical reactions and the limited generation rate of surface reaction products are key factors governing the efficiency of material removal during CMG [33].

Due to the complex coupling of chemical effects and mechanical forces in the CMG process, it is still difficult to directly observe the dynamic atomic-scale reactions that occur at the tool–workpiece interface. Consequently, computational modeling including molecular dynamics (MD) simulation has become a crucial approach for exploring such interfacial phenomena. Researchers have used ReaxFF MD, a reactive molecular dynamics method, to conduct a series of studies on the tribochemical processes involved in the CMP of brittle crystalline materials including monocrystalline silicon, silicon carbide, and diamond. Yuan et al. [34,35] utilized this method to explore the polishing behavior of diamond, revealing how variations in normal load and sliding velocity affect wear, subsurface damage, and atomistic material removal. Their results showed that pressure exerts a stronger effect on atomic-scale removal than sliding velocity. Wen et al. [36,37] examined the CMP of single-crystal silicon using silica-based abrasives in aqueous media, elucidating the atomistic removal mechanisms under such conditions. He et al. [38] studied the effect of introducing ultrasonic vibration to abrasive particles during SiC CMP, focusing on how the vibrational behavior of abrasives influences interfacial chemical reactions and the extent of substrate damage. Yang et al. [39] investigated the chemo-enhanced polishing of 6H-SiC, emphasizing the coupling between mechanical abrasion and surface chemistry during material removal. Zhou et al. [40] analyzed the CMP behavior of 3C-SiC in different media—dry, pure water, and hydrogen peroxide—to clarify how environmental factors govern the efficiency of chemical–mechanical synergy. Overall, ReaxFF MD has demonstrated strong capability in simulating atomic-scale tribochemical behaviors and chemo-mechanical phenomena that take place during CMP and CMG processes.

To further improve the efficiency and precision of solid-state reaction grinding of sapphire, an ultrasonic vibration–assisted solid-state reaction grinding method is proposed. The feasibility of ultrasonic vibration in enhancing solid-state reactions and machining efficiency is evaluated through theoretical analysis and numerical calculations, while the underlying microscale mechanisms are investigated using ReaxFF MD and classical MD simulations. Grinding experiments demonstrate that the introduction of ultrasonic vibration effectively enhances material removal efficiency and surface quality.

2. Analysis of the principle of ultrasonic vibration-assisted solid-state reaction grinding

In CMG, interfacial chemical reactions involving abrasive particles and the substrate material are crucial for achieving material removal. During dry CMG of sapphire using silica-based soft abrasives, a solid-state reaction takes place at the contact region, resulting in the generation of mullite as the reaction product [30]. The Mohs hardness of mullite ranges from 6 to 7, whereas sapphire exhibits a hardness of approximately 9 and silica abrasives around 7. This hardness gradient allows the silica abrasives to preferentially remove the relatively softer reaction layer, thereby facilitating effective material removal from the sapphire surface and yielding a surface with minimal subsurface damage [41]. The interfacial solid-state interaction involving silica abrasives and the sapphire substrate follows an Arrhenius-type relationship that links the reaction rate constant K to temperature:

$$K = A\exp\left(-\frac{\Delta G}{\mathrm{R}T}\right) \tag{1}$$

where ΔG is the activation energy, A is the pre-exponential factor, R is the Boltzmann constant, and T is the temperature.

Mechanically induced chemical reactions are formulated on the basis of transition state theory (reaction rate theory) and find extensive use across research domains including friction, wear, and tribochemistry [42]. The core concept considers the work performed by external forces on the reaction system, which subsequently reduces the activation energy barrier of the reaction [43]. Eq. (2) illustrates the contribution of mechanical work in lowering the reaction energy barrier as:

$$\Delta G_{act} = \Delta G - W \tag{2}$$

where ΔG_{act} is the activation energy considering mechanical work, and W is the work done by external mechanical forces on the reaction system.

The principle of mechanically induced solid-state reaction is illustrated in Fig. 1(c). Based on Eq. (1), the contribution of mechanical work to reducing the reaction energy barrier is considered, where the energy barrier for the mechanically induced chemical reaction is ΔG_{act}. Consequently, the rate equation for the mechanically induced interfacial solid-state reaction can be expressed as Eq. (3), where K_f is the rate constant of the mechanically induced interfacial solid-state reaction. The contribution of mechanical work to the reaction rate is represented by the term $\exp(W/\mathrm{R}T)$. Evidently, the rate of the mechanically induced solid-state chemical reaction increases with enhanced mechanical activation. Moreover, increasing the amount of mechanical work can

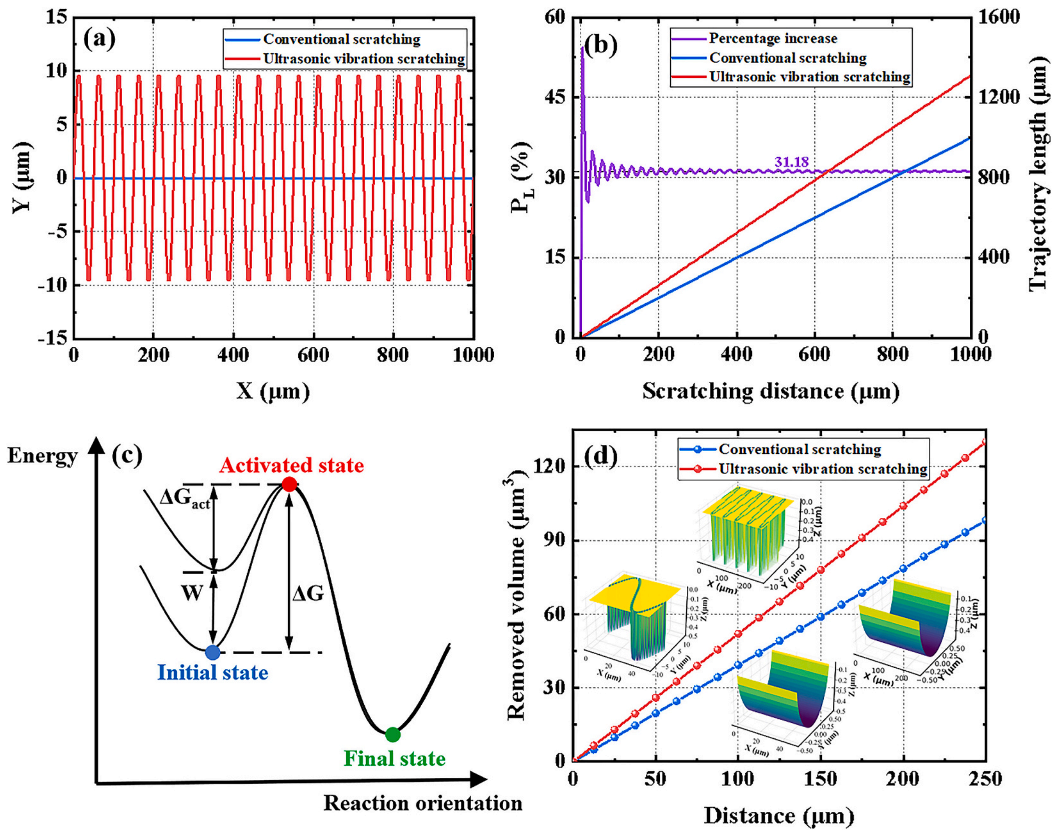

Fig. 1. Comparison between single-grit ultrasonic vibration scratching and conventional scratching: (a) abrasive motion trajectory; (b) trajectory length; (c) mechanism of mechanical-force-promoted interfacial solid-state reaction; (d) material removal volume.

promote the rapid occurrence of the interfacial solid-state reaction.

$$K_f = A\exp\left[-\frac{(\Delta G - W)}{RT}\right] = A\exp\left(\frac{W}{RT}\right)\exp\left(-\frac{\Delta G}{RT}\right) \tag{3}$$

The differences in motion trajectory length, mechanical work, and material removal volume between single-grit ultrasonic vibration and conventional scratching were investigated and compared using numerical methods. This analysis aimed to evaluate the feasibility of introducing an ultrasonic vibration-assisted energy field to enhance the material removal efficiency in CMG. In the numerical calculations, the vibration frequency (f) was set to 20 kHz, the vibration amplitude (A_m) to 10 μm, and the scratching linear velocity (V_s) to 1 m/s, uniformly applied across all simulations.

Conventional scratching trajectory:

$$\begin{cases} x = V_s t \\ y = 0 \end{cases} \tag{4}$$

where x is the displacement along the x-direction, V_s is the scratching velocity, and t is the scratching time.

Therefore, the conventional scratching trajectory length L_{CG} is:

$$L_{CG} = \int_0^T V_s dt \tag{5}$$

Ultrasonic vibration scratching trajectory:

$$\begin{cases} x = V_s t \\ y = A_m sin(2\pi f t) \end{cases} \tag{6}$$

where y is the displacement of the abrasive grain along the y-direction, A_m is the ultrasonic vibration amplitude, and f is the ultrasonic vibration frequency.

Therefore, the ultrasonic vibration scratching trajectory length L_{UV} is:

$$L_{UV} == \int_0^T \sqrt{\left(\frac{dx}{dt}\right)^2 + \left(\frac{dy}{dt}\right)^2} dt = \int_0^T \sqrt{(V_s)^2 + (2\pi A_m f)^2 \cos^2(2\pi f t)} dt \tag{7}$$

The percentage increase in trajectory length P_L for single-grit ultrasonic vibration scratching compared to conventional scratching is expressed as:

$$P_L = 100 \times \left(\frac{L_{UV}}{L_{CG}} - 1\right) = 100 \times \left(\frac{\int_0^T \sqrt{(V_s)^2 + (2\pi A_m f)^2 \cos^2(2\pi f t)}\, dt}{\int_0^T V_s dt} - 1\right) \tag{8}$$

The calculated scratching trajectories for the two scratching modes are shown in Fig. 1(a). The trajectory length increase rate gradually stabilizes over time, with P_L stabilizing at approximately 31.18%, as illustrated in Fig. 1(b). A longer trajectory length implies more frequent interactions of the abrasive grain with the workpiece surface, which promotes interfacial solid-state reactions involving the abrasive and the processed surface. Furthermore, the material removal volume in single-grit scratching is closely related to the trajectory length. Ultrasonic vibration scratching exhibits a longer trajectory length than conventional scratching within the same duration, indicating that UVCMG can remove more material from the reaction-modified surface through abrasive scratching [44]. Based on a material removal model previously established by our research group [45], with the abrasive cutting depth set to 0.5 μm, numerical simulations reveal that the material removal volume under ultrasonic vibration-assisted scratching exceeds that of conventional conditions by approximately 32.5%, as illustrated in Fig. 1 (d).

Let the ratio of the trajectory length of single-grit ultrasonic vibration scratching to that of conventional scratching be denoted as k_L:

$$k_L = \frac{L_{UV}}{L_{CG}} = \frac{\int_0^T \sqrt{(V_s)^2 + (2\pi A_m f)^2 \cos^2(2\pi f t)}dt}{\int_0^T V_s dt} \tag{9}$$

The work performed by the scratching force in single-grit conventional scratching is expressed as:

$$W_{CG} = F_0 \int_0^T V_s dt \tag{10}$$

where F_0 is the average scratching force per cycle in conventional scratching.

The work performed by the scratching force in single-grit ultrasonic vibration scratching is given by:

$$W_{UV} = F_a \int_0^T \sqrt{(V_s)^2 + (2\pi A_m f)^2 \cos^2(2\pi f t)}dt \tag{11}$$

where F_a is the average scratching force per cycle in ultrasonic vibration scratching.

According to previous research conducted by our group, the relationship between the average scratching force per cycle in ultrasonic vibration scratching and conventional scratching is as follows [46]:

$$F_a = \frac{1}{T}\int_0^T F_0 cos\left(tan^{-1}\left(\frac{A_m \omega}{V_s} cos\omega t\right)\right)dt \tag{12}$$

Let the ratio of the average scratching force in single-grit ultrasonic vibration scratching to that in conventional scratching be denoted as k_F:

$$k_F = \frac{F_a}{F_0} = \frac{1}{T}\int_0^T cos\left(tan^{-1}\left(\frac{A_m \omega}{V_s} cos\omega t\right)\right)dt \tag{13}$$

Therefore, the growth rate P_W of the scratching force work in single-grit ultrasonic vibration scratching compared to conventional scratching is:

$$P_W = 100 \times \frac{W_{UV} - W_{CG}}{W_{CG}} = 100 \times \left(\frac{F_a L_{UV}}{F_0 L_{CG}} - 1\right) = 100 \times (k_F \times k_L - 1) \tag{14}$$

Eq. (14) fully accounts for the differences in scratching force and abrasive motion trajectory between single-grit ultrasonic vibration scratching and conventional scratching. Although the average scratching force in ultrasonic vibration scratching is reduced compared to that in conventional scratching, the increased trajectory length effectively enhances the mechanical work performed during the abrasive scratching process. Numerical calculations indicate that the mechanical work in single-grit ultrasonic vibration scratching increases by approximately 2.77% compared to conventional scratching. Related molecular dynamics simulations have yielded conclusions consistent with the numerical calculations presented in this study [47,48]. Analysis combining Eq. (3) and Fig. 1(c) demonstrates that ultrasonic vibration scratching provides additional energy to the interfacial solid-state reaction, effectively promoting a higher reaction rate and facilitating the rapid formation of the surface product layer.

3. Analysis of the ultrasonic vibration-assisted solid-state reaction grinding process

3.1. Molecular dynamics simulation setup

For the ReaxFF MD simulations, based on the observation that the sapphire surface becomes covered with a layer of silica powder during the chemical mechanical grinding process, an interfacial solid-state reaction model was constructed featuring amorphous silica overlying the C-plane of sapphire, as shown in Fig. 2(a). In chemical mechanical grinding, the soft abrasive is harder than the surface reaction products generated during grinding. Therefore, the indenter was simplified as a rigid body. The initial model has a 15 Å gap between the amorphous silica indenter and the sapphire substrate. The model dimensions are 4.75 × 4.95 × 11.7 nm^3, containing 19,910 atoms. The simulation time step was set to 0.25 fs, with a damping constant of 10 fs for temperature control. The ReaxFF potential for Mg/Al/Si/O was used in the

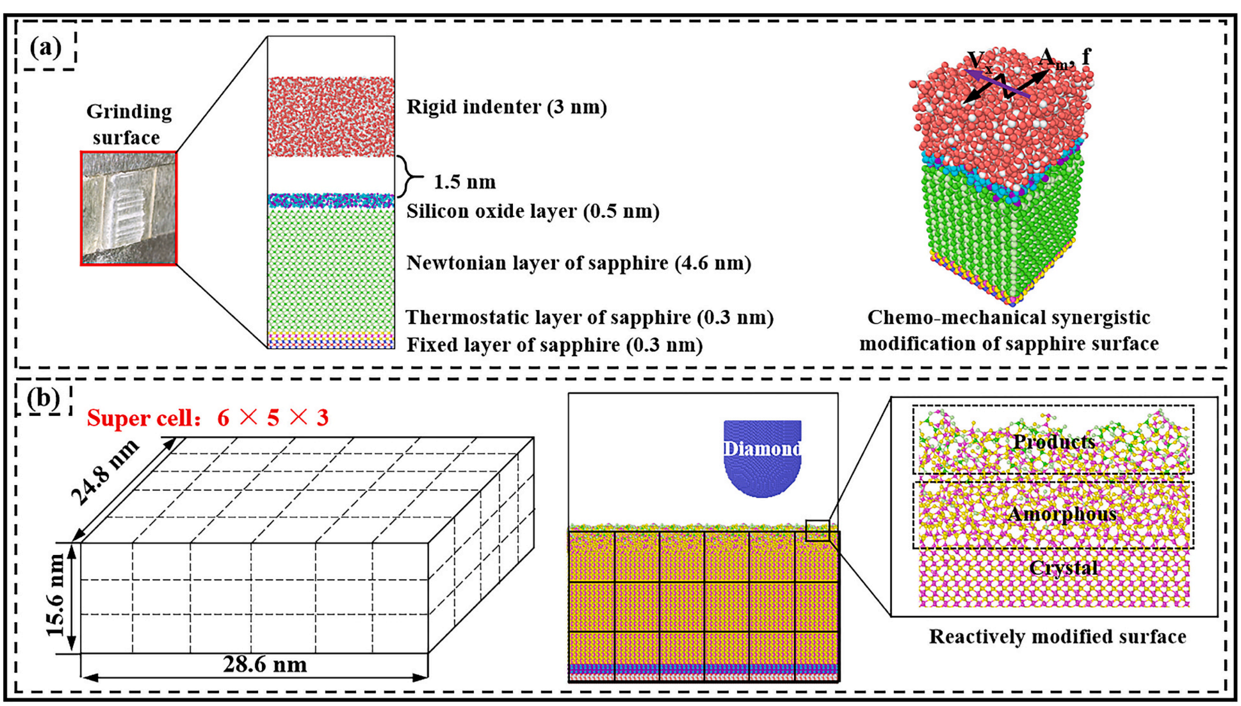

Fig. 2. Solid-state reaction model at the silica soft abrasive-sapphire interface: (a) solid-state reaction interface model, (b) schematic diagram of scratching process, (c) schematic diagram of reaction-modified surface modeling.

simulations [49]. During the scratching process, the number of Si–O–Al bond bridges at the solid-state reaction interface was recorded at intervals of 0.025 Å of scratching distance. The interfacial energy of the solid-state reaction model can reflect the magnitude of work done by external mechanical forces on the reaction interface.

The ReaxFF MD simulation primarily consists of four steps: (1) The model is relaxed at 900 K (above the critical reaction temperature between silica and sapphire) for 20 ps; (2) At 900 K, the indenter is pressed onto the silica surface at a velocity of 100 m/s and then continues to load for an additional 12.5 Å (resulting in a load of approximately 4 GPa); (3) With the indenter maintaining its loaded position, the system undergoes isothermal relaxation for 50 ps to reach full equilibrium; (4) While keeping the indenter at the same depth, scratching is performed with a vibration amplitude of 20 Å and a vibration frequency of 66.67 GHz, moving along the x-direction at 100 m/s over one model period distance of 47.5 Å.

For the classical molecular dynamics (MD) simulations, based on the reaction-modified surface obtained from the ReaxFF MD simulations, a model for single-grit indentation and scratching was constructed, as shown in Fig. 2(b). A sapphire C-plane block model with dimensions of 4.75 × 4.95 × 5.20 nm^3 was first modified using ultrasonic-assisted scratching in ReaxFF MD to obtain the reaction-modified surface. A nanoindentation and scratching model was then established by expanding the cell, with a diamond indenter of 4 nm radius employed. The reaction-modified surface contains 1,379,014 atoms, and the resulting modified sapphire substrate measures approximately 28.6 × 24.8 × 16.6 nm^3. Due to the accumulation of the product layer and amorphous layer, the surface exhibits a protrusion of about 1 nm compared to a perfect surface. Measurements indicate that the product layer has a thickness of 2 nm, and the amorphous layer is 1 nm thick. The potential function developed by Matsui et al. was used to describe atomic interactions in the substrate [50]. This potential has been widely applied in studies on the micromechanisms of elastic-plastic deformation in sapphire [51–54]. Specific potential function parameters are listed in Table 1.

The diamond tip was modeled as a rigid structure. Interatomic forces between carbon atoms of the indenter and those within the substrate were represented using the Lennard–Jones (L–J) potential, a formulation commonly employed in single particle scratching analyses of sapphire [55–57]. The detailed parameters adopted for this potential are summarized in Table 2.

The classical molecular dynamics (MD) simulation process involves three sequential stages: (1) the constructed model undergoes complete relaxation at 300 K for 60 ps to achieve equilibrium; (2) an indenter is driven into the sapphire surface to a penetration depth of 20 Å—equivalent to the thickness of the product layer—at a speed of 25 m/s; and (3) it subsequently performs a scratching motion over a distance of 120 Å along the C-plane at 100 m/s. In the ultrasonic-assisted case, a vibration amplitude of 40 Å and a frequency of 16.67 GHz are applied. The scratching distance over one complete vibration cycle of the indenter is 60 Å, while all other simulation parameters remain consistent with those of conventional scratching.

Table 1
Potential function parameters for the substrate [50].

Interaction	A(eV)	P(Å^2)	C(eVÅ^{-6})	r_c(Å)
Al-Al	31,574,470	0.068	14.07	12
Al-O	28,480	0.172	34.63	
O-O	6463.4	0.276	85.22	
Si-Si	77,127,272,872	0.046	24.30	
Si-O	48,433	0.161	44.67	
Si-Al	706,213,824	0.057	18.15	

Table 2
Parameter settings for the Lennard-Jones potential [55–57].

Interaction	σ(Å)	Ɛ(eV)
Al-C	3.0135	0.035078
O-C	3.195	0.0032918
Si-C	3.629	0.0089465

3.2. Chemo-mechanical synergy induced generation of reaction-modified surface

During CMG, interactions between the compliant abrasive particles and the sapphire substrate trigger chemo-mechanical reactions, leading to the development of a modified surface layer. Transmission electron microscopy (TEM) examinations of sapphire substrates subjected to CMG have revealed the existence of both a reaction product layer and an amorphous zone approximately 10 nm in thickness near the surface [31].

To investigate the atomic-scale evolution of sapphire under these coupled effects, the radial distribution function (RDF) was employed to examine atomic ordering on the surface under conventional scratching conditions. The RDF, denoted as g(r), characterizes the variation of atomic density relative to interatomic spacing r, where g(r) indicates the probability of finding a neighboring atom at distance r [58,59]. As illustrated in Fig. 3(a), the first dominant peak of the RDF curve appears at 1.85 Å, corresponding to the characteristic Al—O bond length in sapphire [60,61]. With increasing scratching displacement, the peak intensity gradually diminishes, suggesting a progressive loss of crystalline order and the development of localized amorphous regions within the surface layer.

After the indenter completes the scratching process, a reaction-modified surface is generated on the sapphire substrate, as shown in Fig. 3(b). The surface modified by chemo-mechanical synergy consists of three distinct layers: a product layer, an amorphous layer, and a single-crystal layer. In this study, the “product layer–amorphous layer” structure is referred to as the reaction-modified surface. The surface structure of sapphire obtained through ReaxFF MD simulations is consistent with the subsurface structure of sapphire substrates observed in chemical mechanical grinding experiments [31]. The softened reaction-modified surface induced by chemo-mechanical synergy on the sapphire surface facilitates further material removal [62].

3.3. Ultrasonic vibration promotes the formation of reaction-modified surfaces

Both conventional scratching and ultrasonic scratching resulted in an increase in interfacial energy. The interfacial energy increased by 0.35% after conventional scratching and by 2.24% after ultrasonic scratching, indicating that ultrasonic scratching provides higher interfacial energy to the solid-state reaction interface, as shown in Fig. 4(a). The number of bond bridges at the solid-state reaction interface increased after both conventional and ultrasonic scratching. After conventional scratching, the number of bond bridges increased by 195.5%, while after ultrasonic scratching, it increased by 350.1%. Compared with conventional scratching, the ultrasonic-assisted process exhibited a 79.1% greater effectiveness in promoting the generation of Si–O–Al bridge bonds at the solid–solid reaction interface. This indicates that ultrasonic vibration scratching facilitates the progression of interfacial solid-state reactions to a greater extent than conventional scratching, as illustrated in Fig. 4 (b).

The application of ultrasonic vibration during scratching injects supplementary energy into the solid-state reaction interface, promoting the creation of additional Si–O–Al bridge bonds within the interfacial region. This added energy accelerates the progress of interfacial reactions and facilitates the rapid development of the product layer. These findings align well with the trends predicted by the mechanically

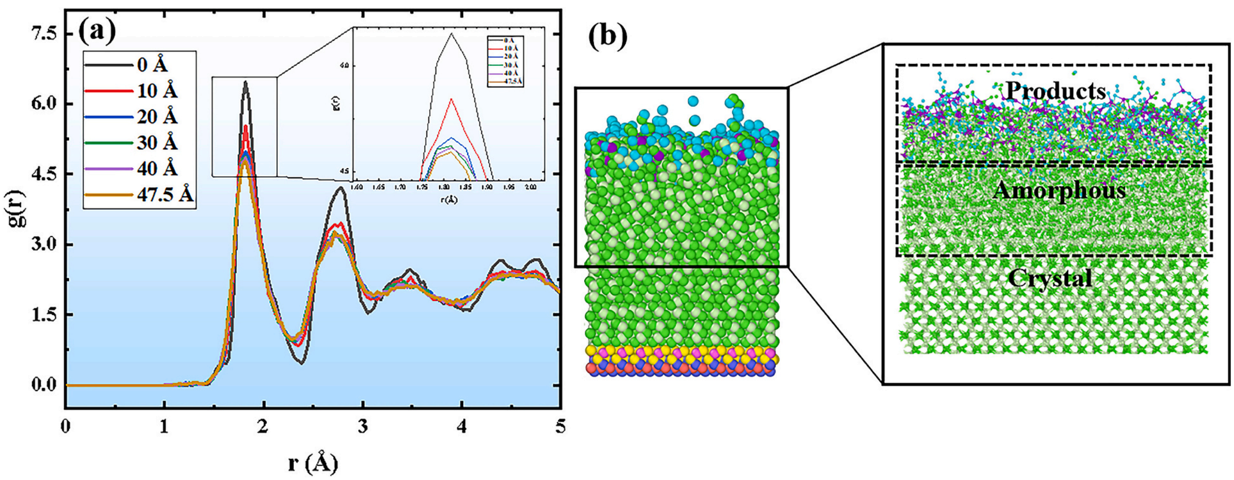

Fig. 3. Structural evolution of the sapphire surface during scratching: (a) radial distribution function curve, (b) microstructure of the reaction-modified surface.

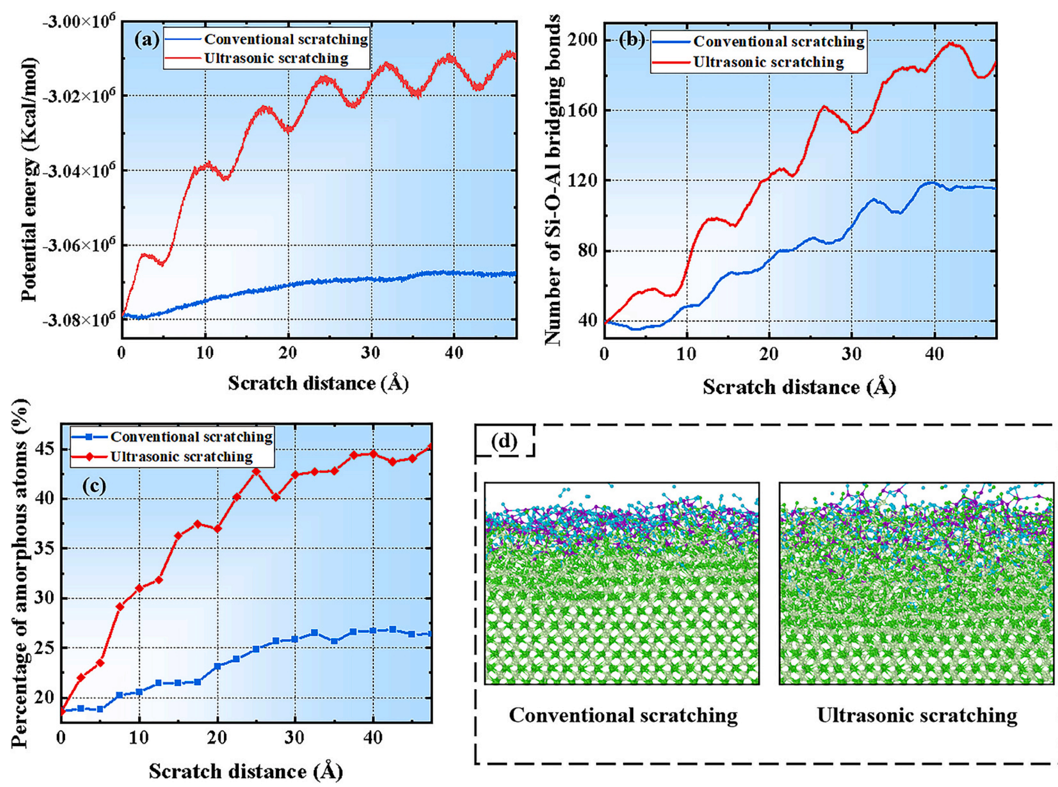

Fig. 4. Enhancement effect of the ultrasonic-assisted energy field on the interfacial solid-state reaction: (a) interfacial energy; (b) number of Si–O–Al bond bridges; (c) percentage of amorphous atoms; (d) obtained reaction-modified surface after scratching.

induced interfacial reaction rate model (Eq. (3)), which suggests that external mechanical work contributes energy to the reaction system, thereby overcoming the activation barrier and increasing the probability and rate of interfacial reactions. Besides the formation of a reaction product layer through surface bonding, the mechanical effects associated with the interfacial reaction also lead to the generation of an amorphous region beneath the product layer. As illustrated in Fig. 4(c) and (d), the production rate of amorphous atoms under ultrasonic vibration surpasses that observed under conventional scratching. When the scratching distance reaches 30 Å, the fraction of amorphous atoms tends to stabilize without further significant growth. Relative to the pristine surface, the proportion of amorphous atoms within the reaction-modified layer rises by 7.78% after conventional scratching and by 26.71% with ultrasonic vibration assistance, representing a 71.73% increase over the conventional case. These results confirm that ultrasonic-assisted scratching substantially enhances both the formation rate and overall concentration of amorphous atoms compared with conventional scratching.

3.4. Ultrasonic vibration enhances material removal from the reaction-modified surface

The microscopic mechanism of material elimination in chemical mechanical grinding involves two main phases: the formation of a reaction-altered layer and its subsequent detachment. Once this altered layer is stripped away, the newly exposed sapphire surface reacts chemically in the solid state with the soft abrasive. These two steps repeat cyclically, ensuring continuous sapphire removal [63]. During ultrasonic scratching, the sapphire substrate experiences a more significant temperature increase than under conventional conditions. This temperature rise correlates directly with the mechanical energy imparted by the abrasive. The greater work input during ultrasonic operation causes the substrate temperature to increase more rapidly [48], as illustrated in Fig. 5(b). When the surface product film is eliminated, the elevated temperature of the substrate promotes faster progress of the following interfacial solid-state reactions. Throughout both the conventional and ultrasonic single-grit scratching tests, the number of atoms detached from the modified surface was tracked. Fig. 5(a) shows that as the scratching distance increases, the quantity of displaced surface atoms also grows, with ultrasonic scratching consistently achieving higher atomic removal. Once the scratching distance exceeds a complete vibration cycle, the enhancement ratio of ultrasonic scratching stabilizes, fluctuating between 137% and 168%. The post-scratching morphologies over a distance of 120 Å for both modes are presented in Fig. 5 (c), confirming that ultrasonic vibration enables more effective elimination of the reacted surface layer.

Compared with traditional scratching, ultrasonic vibration introduces additional energy into the interface, thereby raising the sapphire substrate temperature. The higher temperature encourages interfacial reactions between the freshly revealed sapphire region and the soft abrasive while also expediting the detachment of the reacted layer, allowing quicker exposure of the underlying unreacted substrate. In this way, the ultrasonic-assisted energy field strengthens the recurring removal cycle—from the generation to the elimination of the reaction-modified layer.

4. Experimental study on ultrasonic vibration-assisted solid-state reaction grinding

4.1. Grinding experimental setup

The experimental platform consists of an ultrasonic CNC machine tool, an ultrasonic control system, and a force signal acquisition device. The ultrasonic CNC machine tool, model DY-ULV500, is manufactured by Hangzhou Dayin Ultrasonic Technology Co., Ltd. The ultrasonic control system is integrated into the CNC machine tool and applies one-dimensional ultrasonic vibrations through the machine spindle, with an ultrasonic tool holder model BT30. The force signal acquisition device includes a force measurement plate, data acquisition unit, signal cables, charge amplifiers, and a computer. The force measurement plate, produced by Kistler, works in conjunction with DynoWare software (version 3.1.2.0) to collect grinding force data. As illustrated in the schematic of the grinding setup in Fig. 6, a sapphire piece measuring 10 × 10 × 1 mm^3 (obtained by laser cutting a sapphire C-plane substrate wafer produced by Fujian Jing'an Co., Ltd.) is attached to the fixture platform using heated wax. The fixture platform is securely mounted on the machine tool worktable with screws. A custom-made soft abrasive grinding tool is installed on the ultrasonic tool holder using a collet, and the ultrasonic tool holder is mounted on the machine spindle.

The ultrasonic control system was set to the maximum voltage of 95 V, with the vibration frequency set to the measured resonant frequency of the transducer at 28.46 kHz. The vibration amplitude of the ultrasonic tool holder was approximately 4.5 μm, indicating good performance of the tool holder. Six experimental groups were established, covering both ultrasonic-assisted and traditional machining modes under three distinct processing durations, aiming to compare the performance differences between the two approaches. The experimental setup is summarized in Table 3. The spindle rotated at 2000 rpm, which—given the geometry of the custom-designed grinding head—produced a peripheral velocity of

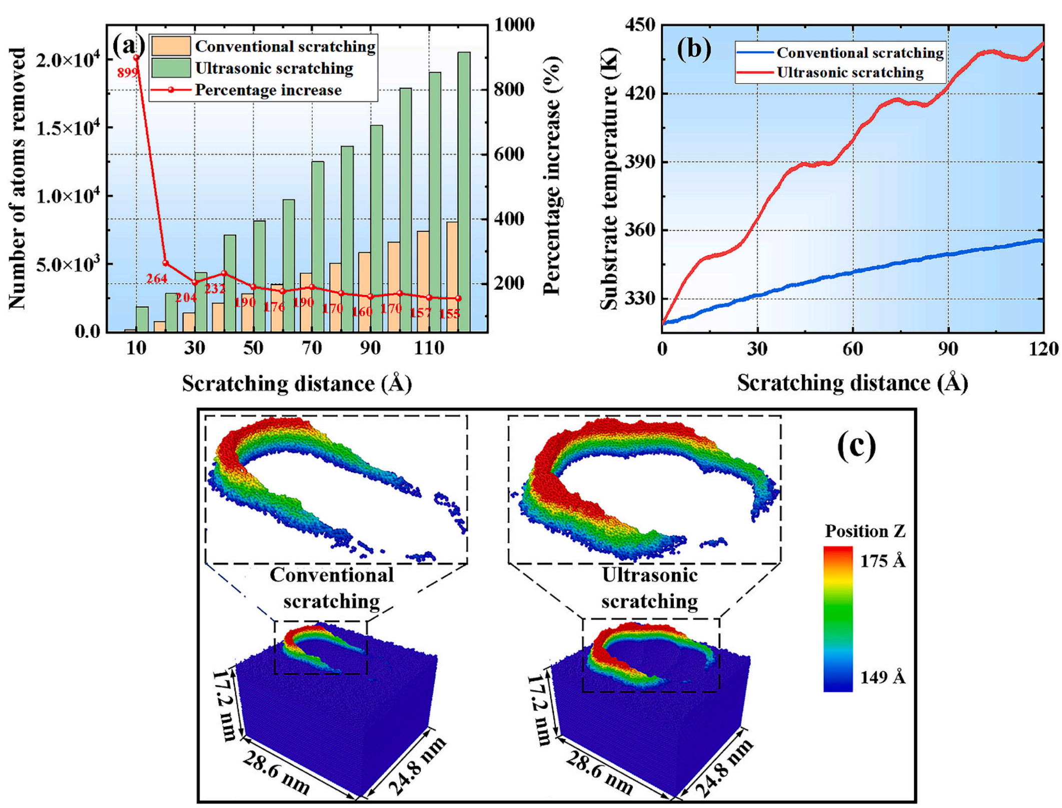

Fig. 5. Comparison between ultrasonic scratching and conventional scratching in the removal of reaction-modified surface material: (a) number of removed surface atoms; (b) substrate temperature; (c) surface morphology after scratching.

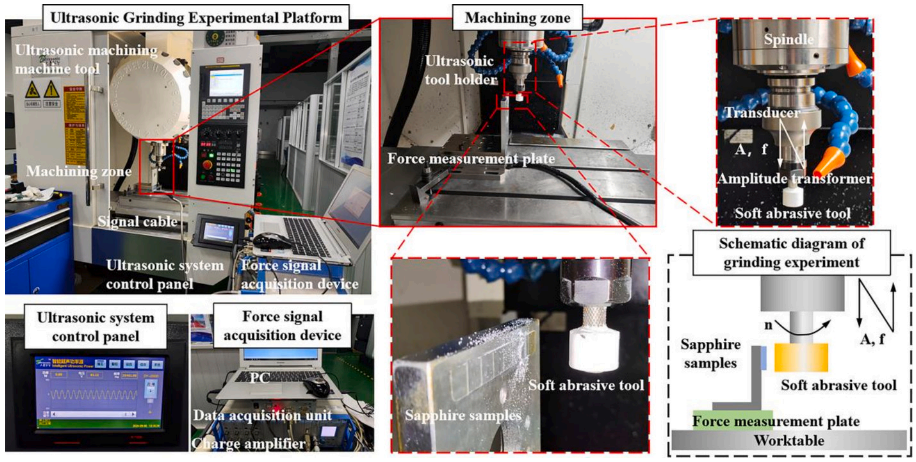

Fig. 6. Ultrasonic vibration-assisted grinding experimental platform.

Table 3
Grinding experiment parameter settings.

Grinding method	Total grinding time	Single grinding duration	Total feed depth	Single feed depth	Spindle speed
CMG	8 min	1 min	40 μm	5 μm	2000 rpm
	16 min	2 min			
	32 min	4 min			
UVCMG	8 min	1 min			
	16 min	2 min			
	32 min	4 min			

approximately 2 m/s. The total grinding depth was 40 μm, achieved in eight steps with a single infeed depth of 5 μm. The three grinding durations were 8 min, 16 min, and 32 min, corresponding to grinding times of 1 min, 2 min, and 4 min, respectively, after each 5 μm depth infeed.

4.2. Analysis of grinding force

As the sapphire surface material is progressively removed and the soft abrasive tool undergoes normal wear, both the dynamic tangential and normal grinding forces gradually decrease with increasing grinding time. The average grinding force is obtained by averaging the dynamic grinding force over the grinding duration. All grinding forces discussed in this section refer to the average values at a feed depth of 40 μm. As shown in Fig. 7(a), the average tangential grinding forces for conventional grinding at durations of 8, 16, and 32 min are 2.83 N, 1.42 N, and 0.73 N, respectively, while those for ultrasonic-assisted grinding are 2.21 N, 1.42 N, and 0.69 N. As shown in Fig. 7(b), the average normal grinding forces for conventional grinding at 8, 16, and 32 min are 5.03 N, 2.99 N, and 1.36 N, respectively, whereas the corresponding values for ultrasonic-assisted grinding are 3.72 N, 2.76 N, and 1.23 N.

With the introduction of the ultrasonic-assisted energy field, both tangential and normal grinding forces decrease. Compared with CMG, UVCMG reduces the average tangential grinding force by 21.91%, 21.13%, and 5.48%, and the average normal grinding force by 26.04%, 7.79%, and 9.56% at the corresponding grinding durations. The reduction in grinding force in ultrasonic-assisted grinding is generally attributed to the extended abrasive trajectories, which enhance the material removal rate and thereby lower the grinding force [64]. In this study, the ultrasonic vibration–assisted energy field further accelerates the solid-state reaction rate between the soft abrasives and the sapphire surface, leading to improved material removal efficiency and consequently reduced grinding forces in UVCMG compared with CMG.

4.3. Analysis of surface roughness

After chemical mechanical grinding, a smooth sapphire surface as

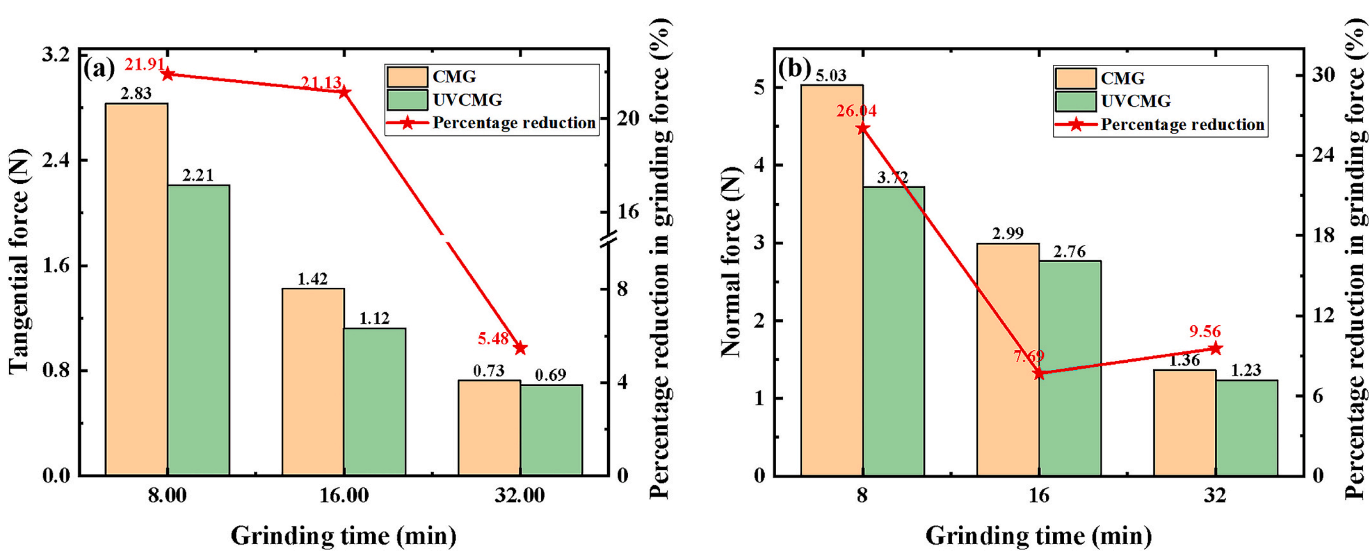

Fig. 7. Comparison of grinding forces between UVCMG and CMG: (a) tangential force; (b) normal force.

shown in Fig. 8(a1)–(a3) can be obtained, indicating that the use of soft abrasive tools enables effective grinding of sapphire surfaces. To quantitatively analyze the machining quality of the sapphire surface after grinding, surface roughness (Sa) measurements were taken at five equally spaced locations within the ground area of the sample.

The initial surface roughness of the sapphire specimen was 278.62 nm. After undergoing CMG for 8, 16, and 32 min, the roughness progressively declined to 97.28 nm, 70.04 nm, and 46.61 nm, indicating a steady enhancement in surface smoothness with longer processing durations. When ultrasonic assistance was applied, the UVCMG process yielded even finer finishes of 79.93 nm, 54.56 nm, and 36.29 nm under the same time intervals. Compared with standard CMG, UVCMG consistently produced smoother surfaces, achieving reductions of 17.84%, 22.10%, and 22.14%, respectively, as shown in Fig. 8(b) and (c). These findings reveal that the sapphire surface topography was significantly refined following material removal, and the introduction of ultrasonic excitation further improved the overall finish. Representative three-dimensional surface profiles obtained from both processing conditions are depicted in Fig. 8(d).

4.4. Analysis of material removal efficiency

Material removal efficiency is as crucial as surface quality in grinding processes, and the material removal efficiency of sapphire CMG is a key focus. A custom-made grinding tool was used to perform CMG at the same location on the sapphire sample to remove surface material. Groove depth measurements were taken at three uniformly distributed points across the machining area, and the groove depths formed within a given duration were employed to assess the efficiency of material removal. The groove depths obtained by CMG were 1.16 μm, 1.58 μm, and 2.92 μm after 8, 16, and 32 min of grinding, respectively. In contrast, the groove depths achieved by ultrasonic-assisted chemical mechanical grinding (UVCMG) under the same conditions were 1.78 μm, 2.01 μm, and 3.22 μm, representing increases of 53.45%, 27.22%, and 10.27%, respectively, compared to conventional CMG, as shown in Fig. 9(a) and (b). Under all three grinding durations, UVCMG resulted in greater material removal than conventional CMG. Increasing the grinding time enhanced material removal, and the introduction of ultrasonic assistance further improved the material removal efficiency of sapphire CMG. The measured groove depth profiles of sapphire samples processed by the two grinding methods are shown in Fig. 9(c1) and (c2). Incorporating ultrasonic assistance enhanced both the surface finish and the removal rate during sapphire CMG.

4.5. Mechanism of ultrasonic-assisted solid-state reaction grinding

The surfaces of the samples before and after chemical mechanical grinding were examined by Raman spectroscopy. The Raman spectrum prior to processing is presented in Fig. 10(a1), displaying three distinct characteristic peaks at 421 cm^{-1}, 579 cm^{-1}, and 751 cm^{-1}, which correspond to vibrational modes associated with the C-plane of sapphire. These results are consistent with existing Raman spectroscopy findings for C-plane sapphire substrates [30,65,66]. The Raman spectrum of the sapphire substrate surface after grinding with a silica soft abrasive tool is shown in Fig. 10(a2). In addition to characteristic peaks similar to those observed before chemical mechanical grinding, two additional characteristic peaks were detected at Raman shifts of 951 cm^{-1} and 1094 cm^{-1}. Comparison with existing literature confirms that these peaks correspond to mullite [67,68]. Furthermore, characteristic peaks were observed at Raman shifts of 1366 cm^{-1} and 1612 cm^{-1}.

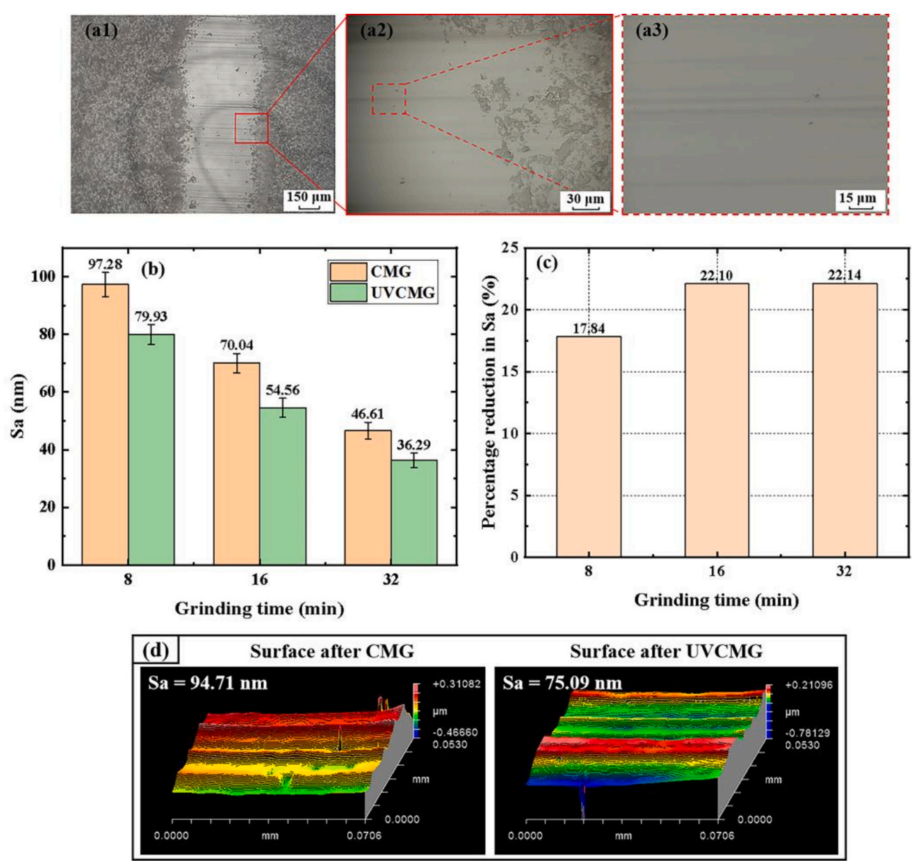

Fig. 8. Surface roughness analysis after chemical mechanical grinding: (a1)–(a3) ground sapphire sample surfaces observed by 3D video microscopy; (b) comparison of surface roughness between conventional grinding and ultrasonic grinding; (c) percentage reduction in surface roughness achieved by ultrasonic grinding; (d) sapphire surfaces after 8 min of conventional grinding and ultrasonic grinding measured by 3D optical profilometry.

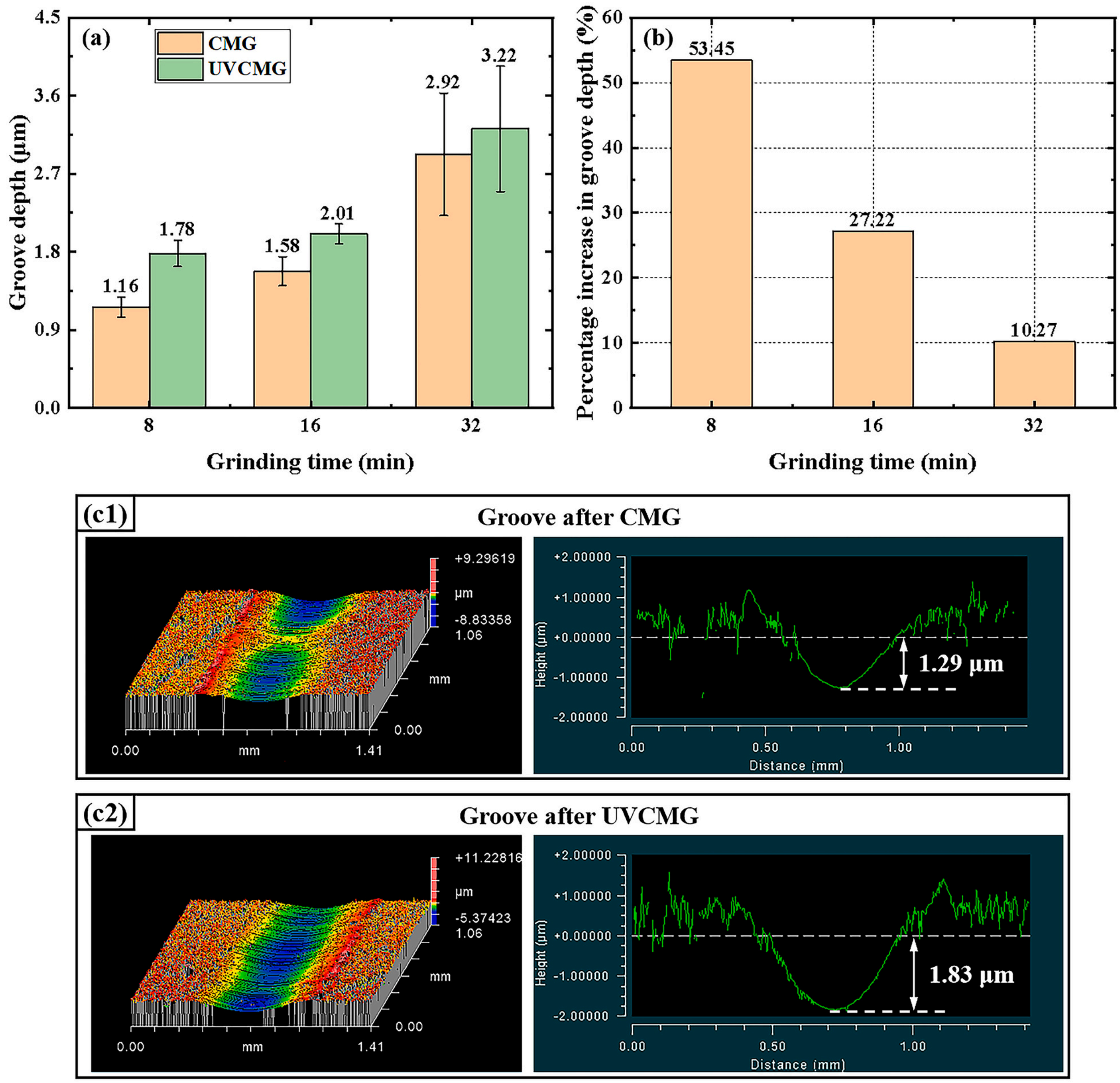

Fig. 9. Comparison of groove depth between conventional grinding and ultrasonic grinding: (a) groove depth; (b) percentage increase in groove depth; (c1)-(c2) groove profiles on sapphire surfaces measured using a 3D optical profiler after 8 min of conventional and ultrasonic grinding.

However, no corresponding substances for these peaks were identified through database comparisons or existing literature.

The surface hardness measured by nanoindentation experiments reflects a material's resistance to localized plastic deformation and helps provide a more comprehensive understanding of its mechanical properties [69]. In general, higher hardness corresponds to stronger resistance to deformation, making the surface material more difficult to be removed by abrasive particles during grinding [70]. The nanoindentation instrument used in this study was manufactured by KLA-TENCOR, model Nano Indenter G200. The continuous stiffness measurement (CSM) method was employed, which enables the determination of hardness as a function of penetration depth [71,72]. The measured hardness values of the pristine sapphire surface and the reaction-modified surface are shown in Fig. 10(b1) and (b2). After the indenter penetrates to a depth of 40 nm, the hardness values tend to stabilize. The hardness of the reaction-modified surface is lower than that of the pristine surface. By averaging the hardness values beyond an indentation depth of 40 nm, the surface hardness of the pristine sapphire is determined to be 38.97 GPa, which is in good agreement with the previously reported value of 39.82 GPa [54]. The nanoindentation results show that the hardness of the reaction-modified surface is 30.80 GPa. Compared with the pristine sapphire surface, the hardness of the sapphire substrate after chemical mechanical polishing decreases by 20.96%.

Conventional CMG generally involves four successive phases: mechanical interaction, preliminary formation of a reaction product layer, creation of a chemically modified surface, and its subsequent elimination [63]. The introduction of an ultrasonic vibration–assisted energy field plays an essential role in promoting interfacial chemical transformation while enhancing the mechanical detachment of surface materials. Ultrasonic scratching injects supplementary energy into the reaction interface, facilitating the interfacial reaction process and leading to a greater generation of amorphous surface atoms, which expedites the development of the modified layer. The altered layer, composed of the product and amorphous regions, exhibits degraded mechanical strength, making it easier to remove in later stages [62].

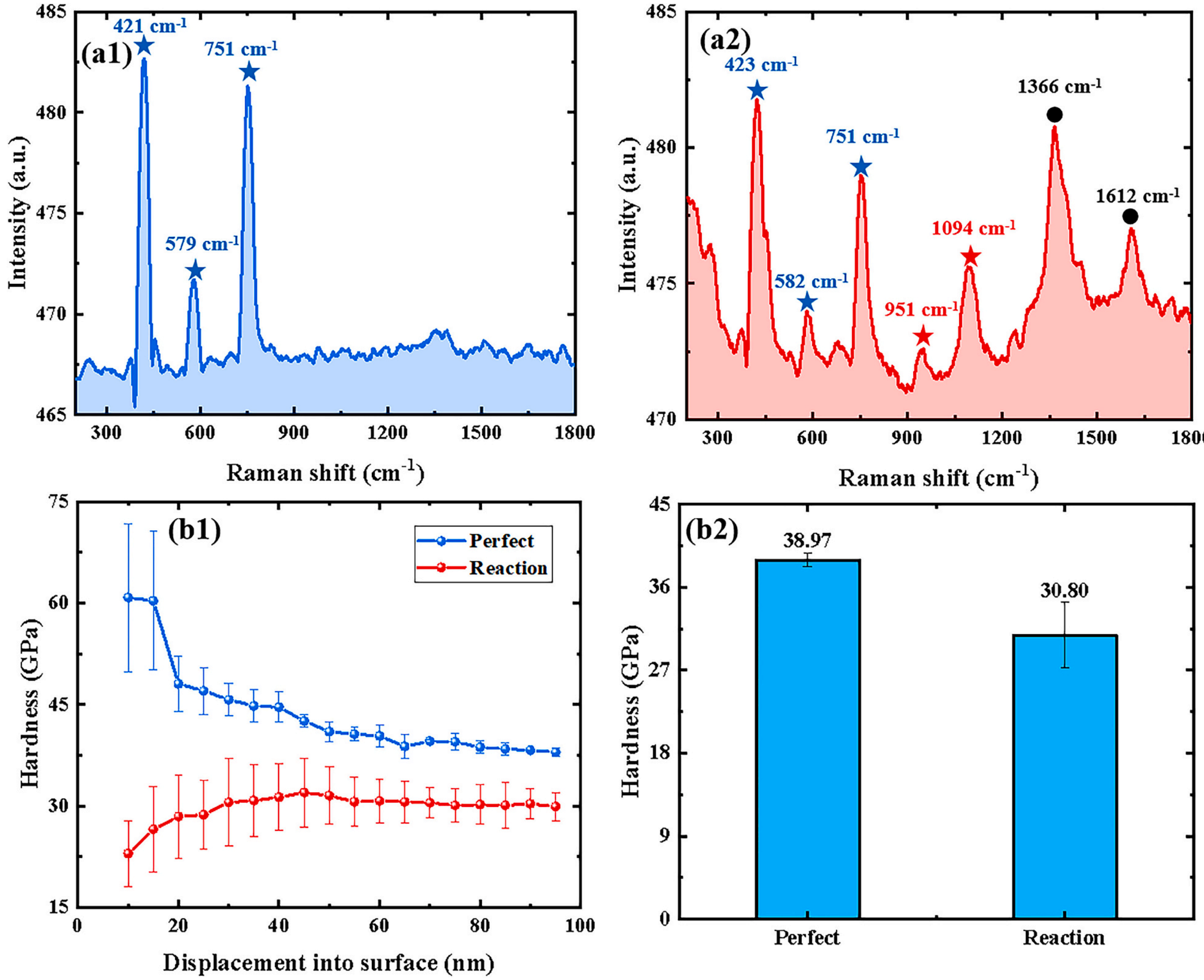

Fig. 10. Composition and mechanical property characterization of the sapphire surface: (a1) Raman spectra before grinding; (a2) Raman spectra after grinding; (b1) Variation of surface hardness with loading depth; (b2) Hardness of the sapphire surface.

During ultrasonic scratching, more surface atoms are displaced within the same duration, accelerating both the elimination of the modified surface and the exposure of new sapphire regions. These freshly uncovered sapphire surfaces promptly interact with the soft abrasives, forming new reaction-modified layers. As depicted in Fig. 11, the mechanism of ultrasonic-assisted CMG reveals that the applied energy field accelerates the cyclic transition from layer formation to removal, thereby improving overall processing efficiency.

The role of the ultrasonic vibration–assisted energy field differs between ultrasonic-assisted grinding and UVCMG. In conventional grinding, where the main challenge is balancing machining precision and efficiency, ultrasonic vibration reduces the surface roughness (Ra) of sapphire by 5.19%–9.56% and decreases the pit depth from 12.83 μm to 9.27 μm (27.75%), which contributes to improved material removal efficiency, mainly by modifying abrasive trajectories and reducing grinding forces and subsurface damage [73]. In contrast, in CMG, a high-precision process whose main limitation is the low material removal rate due to the slow interfacial solid-state reaction, the introduction of ultrasonic vibration has a more pronounced effect, reducing surface roughness by 17.84%–22.14% and increasing material removal by 10.27%–53.45%. This indicates that ultrasonic vibration significantly accelerates interfacial reactions in UVCMG, thereby enhancing material removal efficiency while maintaining high surface quality.

5. Conclusions

This study proposes an ultrasonic vibration–assisted chemical mechanical grinding (UVCMG) method and establishes a direct mechanism–performance correlation through combined molecular dynamics simulations and grinding experiments. Simulations demonstrate that ultrasonic vibration elevates the interfacial energy state, thereby accelerating solid-state reactions, strengthening interfacial bonding, and promoting the rapid detachment of reaction-modified atoms, which collectively intensify the “reaction–removal” cycle. These mechanistic effects are directly reflected in the experimental results, where UVCMG achieves a reduction in surface roughness of 17.84%–22.14%, an increase in material removal efficiency of 10.27%–53.45%, and a noticeable decrease in both tangential and normal grinding forces compared with conventional CMG. The strong agreement between simulation and experiment confirms that ultrasonic vibration enhances reaction kinetics, facilitates material removal, and reduces grinding forces, establishing UVCMG as an effective and innovative strategy for high-efficiency, high-quality machining of sapphire and other hard and brittle materials. Future work will focus on further process optimization and systematic investigations to accelerate the practical application of this method.

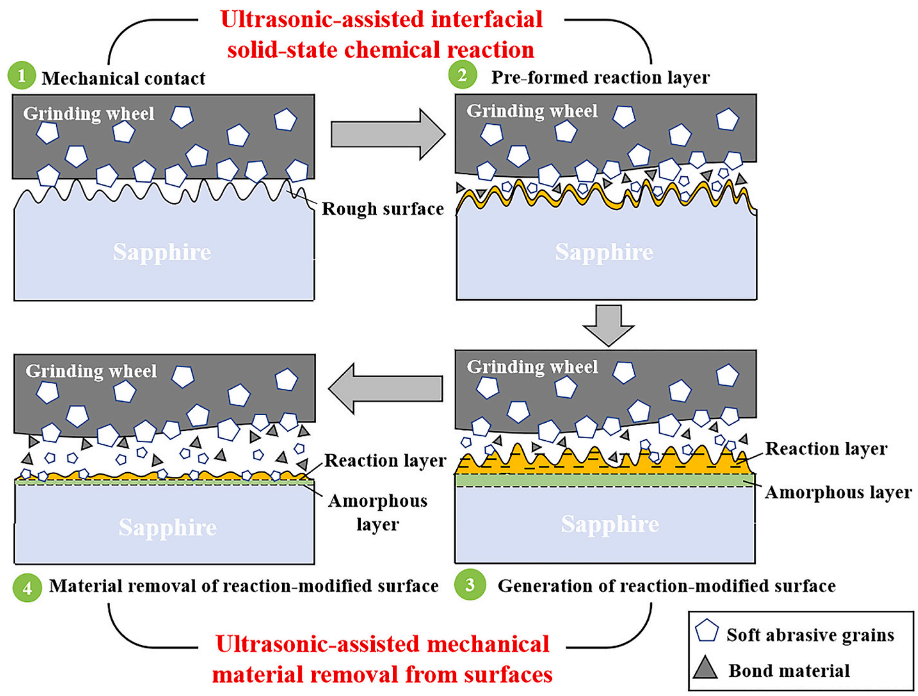

Fig. 11. Mechanism of ultrasonic-assisted chemical mechanical grinding.

CRediT authorship contribution statement

Gen Chen: Writing – original draft, Software, Methodology, Data curation, Conceptualization. **Zhongwei Hu:** Writing – review & editing, Supervision, Funding acquisition, Conceptualization. **Kun Shi:** Methodology, Data curation. **Yuqiang Zhang:** Writing – review & editing, Methodology. **Xintian Cai:** Writing – review & editing, Methodology. **Qing Peng:** Supervision, Resources, Funding acquisition.

Declaration of Generative AI and AI-assisted technologies in the writing process

During the preparation of this work the authors used DeepSeek in order to have English grammar corrected. After using this tool/service, the authors reviewed and edited the content as needed and take full responsibility for the content of the published article.

Declaration of competing interest

The authors declare that they have no known competing financial interests or personal relationships that could have appeared to influence the work reported in this paper.

Acknowledgement

This work was supported by the National Natural Science Foundation of China (Grant No. 52175404, 12272378).

References

[1] Akselrod MS, Bruni FJ. Modern trends in crystal growth and new applications of sapphire. J Cryst Growth 2012;360:134–45.
[2] Katyba GM, Zaytsev KI, Dolganova IN, et al. Sapphire shaped crystals for waveguiding, sensing and exposure applications. Prog Cryst Growth Charact Mater 2018;64(4):133–51.
[3] Dobrovinskaya ER, Lytvynov LA, Pishchik V. Sapphire: material, manufacturing, applications[M]. In: Sapphire: Material, Manufacturing, Applications; 2009.
[4] Wang G, Zuo H, Zhang H, et al. Preparation, quality characterization, service performance evaluation and its modification of sapphire crystal for optical window and dome application. Mater Des 2010;31(2):706–11.
[5] Wang S, Zhang Q, Zhao Q, et al. Investigate on surface/subsurface damage mechanisms and manufacturability of ultra-smooth surface in ultra-precision ductile grinding of sapphire optics. J Mater Res Technol 2025;34:1966–89.
[6] Su Z, Liang Z, Ma Y, et al. Influence of surface damage on the optical properties of sapphire and its etching repair method. Ceram Int 2024;50(7, Part A):10034–54.
[7] Bussière B, Sanner N, Sentis M, et al. Importance of surface topography on pulsed laser-induced damage threshold of sapphire crystals. Sci Rep 2017;7(1):1249.
[8] Wang L, Hu Z, Chen Y, et al. Material removal mechanism of sapphire substrates with four crystal orientations by double-sided planetary grinding. Ceram Int 2020;46(6):7813–22.
[9] Yin T, Du H, Zhang G, et al. Theoretical and experimental investigation into the formation mechanism of surface waviness in ultra-precision grinding. Tribol Int 2023;180:108269.
[10] Suetomi T, Kakinuma Y, Fukuta M, et al. Influence of servo characteristics on crack generation in ultra-precision grinding of optical glass lenses. Procedia CIRP 2018;77:130–3.
[11] Wan L, Dai P, Li L, et al. Investigation on ultra-precision lapping of A-plane and C-plane sapphires. Ceram Int 2019;45(9):12106–12.
[12] Wang S, Wang S, Zhao Q. Subsurface damage in sapphire ultra-precision grinding. J Manuf Process 2024;129:215–37.
[13] Wang S, Zhao Q, Yang X. Surface and subsurface microscopic characteristics in sapphire ultra-precision grinding. Tribol Int 2022;174:107710.
[14] Wang S, Sun G, Zhao Q, et al. Monitoring of ductile–brittle transition mechanisms in sapphire ultra-precision grinding used small grit size grinding wheel through force and acoustic emission signals. Measurement 2023;210:112557.
[15] Wang S, Sun G, Zhao Q, et al. Evaluation of grinding characteristics for sapphire ultra-precision grinding using small grit sizes wheels based on AE signals. J Manuf Process 2023;90:94–110.
[16] Zhou M, Cheng Y, Zhong M, et al. Macro and micro-nano machining mechanism for ultrasonic vibration assisted chemical mechanical polishing of sapphire. Appl Surf Sci 2023;640:158343.
[17] Luo Z, Zhang Z, Zhao F, et al. Advanced polishing methods for atomic-scale surfaces: a review. Mater Today Sustain 2024;27:100841.
[18] Zhang Z, Yan W, Zhang L, et al. Effect of mechanical process parameters on friction behavior and material removal during sapphire chemical mechanical polishing. Microelectron Eng 2011;88(9):3020–3.
[19] Xie WX, Zhang ZY, Liao LX, et al. Green chemical mechanical polishing of sapphire wafers using a novel slurry. Nanoscale 2020;12(44):22518–26.
[20] Zhang ZY, Liu J, Hu W, et al. Chemical mechanical polishing for sapphire wafers using a developed slurry. J Manuf Process 2021;62:762–71.
[21] Luo Q, Lu J, Xu X, et al. Removal mechanism of sapphire substrates (0001, 1120 and 1010) in mechanical planarization machining. Ceram Int 2017;43(18):16178–84.
[22] Zhou L, Kawai S, Honda M, et al. Research on chemo-mechanical-grinding (CMG) of Si wafer 1st report: development of CMG wheel. J Japan Soc Precis Eng 2002;68(12):1559–63.
[23] Gao S, Dong ZG, Kang RK, et al. Design and evaluation of soft abrasive grinding wheels for silicon wafers. Proc Inst Mech Eng B J Eng Manuf 2013;227(B4):578–86.

[24] Tian YB, Zhou L, Shimizu J, et al. Elimination of surface scratch/texture on the surface of single crystal Si substrate in chemo-mechanical grinding (CMG) process. Appl Surf Sci 2009;255(7):4205–11.
[25] Zhang Y, Kang R, Ren J, et al. Mechanical effect of abrasives on silicon surface in chemo-mechanical grinding. Int J Mech Sci 2023;257:108544.
[26] Kang R, Gao S, Jin Z, et al. Study on grinding performance of soft abrasive wheel for silicon wafer. Key Eng Mater 2009;416:529–34.
[27] Zhang Yu, Renke Kang, Shang Gao, et al. Development and evaluation of soft abrasive grinding wheel for silicon wafer in wet mechanical chemical grinding. J Mech Eng 2023;59(3):328–36.
[28] Wu KY, Naoki Ebina, Yutaro Zhou, Li Bo Shimizu, Jun Onuki, Teppei Ojima, et al. Study on sapphire wafer grinding by chromium oxide (Cr_2O_3) wheel. Adv Mat Res 2016;1136:311–6.
[29] Wang J. Study on high efficiency lapping of sapphire wafer based on solid phase Tribochemical reaction[D]. Zhejiang University of Technology; 2020.
[30] Wu K, Zhou LB, Onuki T, et al. Study on the finishing capability and abrasives-sapphire interaction in dry chemo-mechanical-grinding (CMG) process. Precision Eng J Int Soc Precis Eng Nanotechnol 2018;52:451–7.
[31] Wu K, Touse D, Zhou LB, et al. Chemo-mechanical grinding by applying grain boundary cohesion fixed abrasive for monocrystal sapphire. Precision Eng J Int Soc Precis Eng Nanotechnol 2021;70:110–6.
[32] Wu K, Zhou LB, Shimizu J, et al. Study on the potential of chemo-mechanical-grinding (CMG) process of sapphire wafer. Int J Adv Manuf Technol 2017;91(5–8): 1539–46.
[33] Vovk EA, Budnikov AT, Dobrotvorskaya MV, et al. Mechanism of the interaction between Al_2O3 and SiO_2 during the chemical-mechanical polishing of sapphire with silicon dioxide. J Surf Investig-X-Ray Synchrotron Neutron Tech 2012;6(1): 115–21.
[34] Yuan S, Guo X, Mao Q, et al. Effects of pressure and velocity on the interface friction behavior of diamond utilizing ReaxFF simulations. Int J Mech Sci 2021; 191:106096.
[35] Yuan S, Guo X, Lu M, et al. Diamond nanoscale surface processing and tribochemical wear mechanism. Diamond Relat Mater 2019;94:8–13.
[36] Wen JL, Ma TB, Zhang WW, et al. Atomistic mechanisms of Si chemical mechanical polishing in aqueous H2O2: ReaxFF reactive molecular dynamics simulations. Comput Mater Sci 2017;131:230–8.
[37] Wen J, Ma T, Zhang W, et al. Atomic insight into tribochemical wear mechanism of silicon at the Si/SiO_2 interface in aqueous environment: molecular dynamics simulations using ReaxFF reactive force field. Appl Surf Sci 2016;390:216–23.
[38] He Y, Tang W, Gao P, et al. Nano-polishing characteristics in vibration-assisted CMP of single-crystal silicon carbide via molecular dynamics simulations. Mater Sci Semicond Process 2023;164:107637.
[39] Yang S, Li X, Zhao Y, et al. MD simulation of chemically enhanced polishing of 6H-SiC in aqueous H_2O_2. J Manuf Process 2023;107:515–28.
[40] Zhou Y, Huang Y, Li J, et al. Investigation of the chemical action mechanism based on reactive force field in SiC chemical–mechanical polishing process. Appl Surf Sci 2024;646:158927.
[41] Shi X, Pan G, Zhou Y, et al. A study of chemical products formed on sapphire (0001) during chemical–mechanical polishing. Surf Coat Technol 2015;270: 206–20.
[42] Chen L, Wen JL, Zhang P, et al. Nanomanufacturing of silicon surface with a single atomic layer precision via mechanochemical reactions. Nat Commun 2018;9.
[43] Spikes H. Stress-augmented thermal activation: tribology feels the force. Friction 2018;6(1):1–31.
[44] Hu Z, Chen Y, Lai Z, et al. AAC theory for ultrasonic vibration-assisted grinding. Int J Adv Manuf Technol 2024;133(3):1609–20.
[45] Chen G, Hu Z, Wang L, et al. Modeling of material removal rate for the fixed-abrasive double-sided planetary grinding of a sapphire substrate. Materials 2024; 17(19):4740.
[46] Zhang Y, Hu Z, Chen Y, et al. Insights into scratching force in axial ultrasonic vibration-assisted single grain scratching. J Manuf Process 2024;112:150–60.
[47] Chen Y, Hu Z, Jin J, et al. Molecular dynamics simulations of scratching characteristics in vibration-assisted nano-scratch of single-crystal silicon. Appl Surf Sci 2021;551:149451.
[48] Xu W, Sheng C, Zhong M. Effects of ultrasonic vibration on sapphire polishing investigated by molecular dynamics. Tribol Int 2022;176:107911.
[49] Yeon J, Chowdhury SC, Daksha CM, et al. Development of Mg/Al/Si/O ReaxFF parameters for magnesium aluminosilicate glass using an artificial neural network-assisted genetic algorithm. J Phys Chem C 2021;125(33):18380–94.
[50] O3-Sio C-M-A, Matsui M. A transferable interatomic potential model for crystals and melts in the system CaO-MgO-Al_2O_3-SiO_2. Mineral Mag 1994;58:571–2.
[51] Chen J, Qi Y, Liu D, et al. Alternate activation-annihilation of dislocations realizes the plasticity of sapphire during indentation. Mater Des 2024;239:112772.
[52] Lin J, Jiang F, Wen Q, et al. Deformation anisotropy of nano-scratching on C-plane of sapphire: A molecular dynamics study and experiment. Appl Surf Sci 2021;546: 149091.
[53] Lin J, Jiang F, Xu X, et al. Molecular dynamics simulation of nanoindentation on c-plane sapphire. Mech Mater 2021;154:103716.
[54] Qiu T, Jiang F, Wang N, et al. Atomistic understanding of the variable nano-hardness of C-plane sapphire considering the crystal anisotropy. J Mater Res Technol 2024;29:4514–25.
[55] Kim WK, Kim BH. A molecular dynamics study on atomistic mechanisms of nano-scale cutting process of sapphire. J Mech Sci Technol 2017;31(9):4353–62.
[56] Kim WK, Xi D, Kim BH. Nanoscale indentation and scratching tests of single crystal sapphire using molecular dynamics simulation. Comput Mater Sci 2019;170: 109195.
[57] Pan D, Li J, Voon LCLY, et al. Determination of Lennard-Jones potential parameters for interfacial interaction in elemental layered crystals. J Appl Phys 2024;135(20): 204301.
[58] Ma Y, Zhang S, Wang T, et al. Atomic diffusion behavior near the bond interface during the explosive welding process based on molecular dynamics simulations. Mater Today Commun 2022;31:103552.
[59] Wang C-L, Wang Q-Y, Zhang Y, et al. Molecular dynamics study of cascade damage at SiC/C interface. Acta Phys Sin 2014;63(15). 153402–153402.
[60] Zhang L, Zhang R, Yang B, et al. Adsorption configuration of AlN on sapphire surface using first-principles calculations. Appl Surf Sci 2021;562:150163.
[61] Choi M, Janotti A, Van De Walle CG. Native point defects and dangling bonds in α-Al_2O_3. J Appl Phys 2013;113(4):044501.
[62] Gao S, Li H, Huang H, et al. Grinding and lapping induced surface integrity of silicon wafers and its effect on chemical mechanical polishing. Appl Surf Sci 2022; 599:153982.
[63] Yinghui Ren, Jiaheng Zhou, Li Wei, et al. Research status and prospect of CMG technology. China Mech Eng 2021;32(18):2143–52.
[64] Jin J, Zhao M, Mao J, et al. Iterative modeling of grain size and force during ultrasonic vibratory–assisted grinding SiCp/Al composites. Int J Adv Manuf Technol 2025;138(7):3559–74.
[65] Wang X, Zheng W, Bao X, et al. Investigation of anisotropic characteristics in ultra-precision grinding of sapphire crystal planes and strategies for suppression. J Manuf Process 2025;133:55–85.
[66] Kadleíková M, Breza J, Veselý M. Raman spectra of synthetic sapphire. Microelectron J 2001;32(12):955–8.
[67] Xu YC, Lu J, Xu XP. The research of reactivity between nano-abrasives and sapphire during polishing process. Integr Ferroelectr 2015;159(1):41–8.
[68] Riedel R, Toma L, Fasel C, et al. Polymer-derived mullite–SiC-based nanocomposites. J Eur Ceram Soc 2009;29(14):3079–90.
[69] Bhushan B. Nano- to microscale wear and mechanical characterization using scanning probe microscopy. Wear 2001;251(1):1105–23.
[70] Xie X, Peng Q, Chen G, et al. Femtosecond laser modification of silicon carbide substrates and its influence on CMP process. Ceram Int 2021;47(10, Part A): 13322–30.
[71] Van Der Rest A, Idrissi H, Henry F, et al. Mechanical behavior of ultrathin sputter deposited porous amorphous Al_2O_3 films. Acta Mater 2017;125:27–37.
[72] Oliver WC, Pharr GM. Measurement of hardness and elastic modulus by instrumented indentation: advances in understanding and refinements to methodology. J Mater Res 2004;19(1):3–20.
[73] Chen Y, Hu Z, Yu Y, et al. Processing and machining mechanism of ultrasonic vibration-assisted grinding on sapphire. Mater Sci Semicond Process 2022;142: 106470.